Thin-Film Bulk Acoustic Resonators and Filters Using ZnO and Lead–Zirconium–Titanate Thin Films

Qing-Xin Su, Paul Kirby, Eiju Komuro, Masaaki Imura, Qi Zhang, and Roger Whatmore

***Abstract*—This paper presents the findings of a design, modeling, and fabrication study of ZnO and $PbZr_{0.3}Ti_{0.7}O_3$ thin-film bulk acoustic resonators and filters. Measurements of the high-frequency responses of ZnO resonators having different area are used to develop an acoustic model that accurately represents resonator impedance data. The models are also used to interpret S-parameter measurements on thin-film $PbZr_{0.3}Ti_{0.7}O_3$-based resonators and a value for the effective coupling coefficient deduced. ZnO and $PbZr_{0.3}Ti_{0.7}O_3$ ladder filters were designed based on measured impedance data from single resonators. Ladder filters based on $PbZr_{0.3}Ti_{0.7}O_3$ have been fabricated for the first time. It is shown that the high coupling coefficient in $PbZr_{0.3}Ti_{0.7}O_3$ leads to bandwidths in the range 100∼120 MHz at a center frequency of 1.6 GHz, larger than the bandwidths of ZnO-based filters.**

***Index Terms*—Acoustic modeling, FBAR, FBAR filters, mobile communications, PZT, thin-film bulk acoustic resonator.**

I. Introduction

MOBILE phones are one of the major driving forces for advancement in miniature electronics. New types of advanced wireless transceivers are entering the commercial market to meet the requirement of voice, data, and multimedia communications. With the development of very large scale integration (VLSI) and digital technology, tremendous improvement has taken place in the miniaturization of wireless communication subsystems. However, there seems to be little room for improvement in the miniaturization of the established surface acoustic wave (SAW) and ceramic devices used for front-end RF filters, IF filters, and voltage-controlled oscillators (VCOs) since they are very difficult to fabricate on-chip. Thin-film bulk acoustic resonator (FBAR) technology represents a breakthrough in miniaturization of frequency-selective devices. If FBAR devices of sufficient performance can be fabricated, they will be the best choice to replace the current ceramic or SAW devices due to their compactness and good compatibility with high-frequency Si or GaAs integrated-circuit (IC) processing [1].

Manuscript received November 7, 2000; revised January 15, 2001.

Q.-X. Su was with the Nanotechnology and Microsystems Group, School of Industrial and Manufacturing Sciences, Cranfield University, Cranfield, Bedford MK43 0AL, U.K. He is now with Philips Research East Asia-Xi'an, Xi'an 710075, China.

P. Kirby, Q. Zhang, and R. Whatmore are with the Nanotechnology and Microsystems Group, School of Industrial and Manufacturing Sciences, Cranfield University, Cranfield, Bedford MK43 0AL, U.K.

E. Komuro and M. Imura are with the Telecom Technology Development Centre, TDK Corporation, Chiba, 272-8558 Japan.

Publisher Item Identifier S 0018-9480(01)02902-7.

TABLE I
MATERIAL PROPERTIES OF CANDIDATE PIEZOELECTRIC MATERIALS FOR FBAR (DATA TAKEN FROM [2])

Materials	AlN	ZnO	PZT
Acoustic velocity (m/s)	10400	6340	4500
Electro-mechanical coupling coefficient κ_t^2	2.89%	7.84%	20.25%
Dielectric constant ε_r	8.5	8.8	350

Candidate piezoelectric materials for FBARs and the material properties that determine the operating frequency, bandwidth, and size of an FBAR element are listed in Table I [2]. To date, AlN and ZnO thin films have been used successfully as the piezoelectric layer in FBARs [1], [3] and a range of filter configurations have been investigated. AlN and ZnO FBAR devices have material properties that make them suitable for current front-end filters for global positioning system (GPS) receivers and RF components in current personal communications system (PCS) handsets, such as duplexers, and VCOs. However, the low electromechanical coupling in AlN and ZnO leads to low-bandwidth filters, making it difficult to meet the requirement for broad-band access and large data transmission in future mobile phones.

Ferroelectric materials in the $PbZr_{1-x}Ti_xO_3$ (PZT) series can have high electromechanical coupling coefficients [4]. In recent years, there has been increasing research activity in the fabrication of ferroelectric films due to the increased commercial interest in nonvolatile memory and "micro"electromechanical devices [5]. The use of thin films rather than ceramic PZT technology can offer fully "integrated" device manufacture with the active PZT layer integrated directly onto a silicon substrate. In this way, there is the potential to increase manufacturing speed and decrease costs. For direct integration with silicon or gallium–arsenide circuits, the low processing temperatures obtained when the "sol-gel" PZT processing route is used to prepare PZT thin films is a great advantage. In this paper, we report on the design, fabrication, and performance of $PbZr_{0.3}Ti_{0.7}O_3$ FBAR resonators and ladder filters.

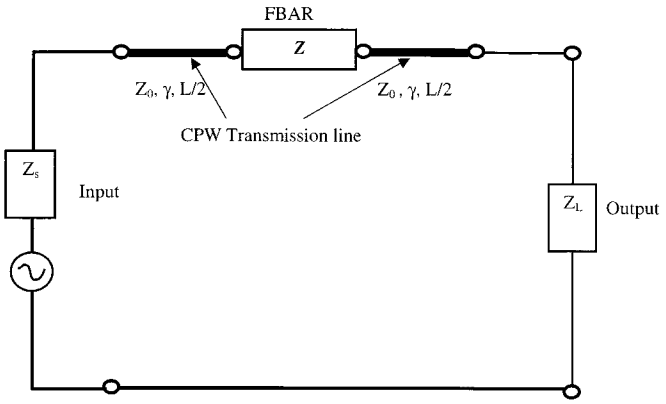

Fig. 1. Equivalent circuit used to model an FBAR embedded in a CPW.

II. FBARS AS BASIC BUILDING BLOCKS FOR FILTERS

A single FBAR is the basic building block of an FBAR filter. There are two reasons for performing in-depth analysis of FBAR structures: to understand the material properties that limit the performance so that they can be optimized, and to be able to model their performance to give parameters that can be used in filter design. Three types of FBAR structures have previously been investigated [1]. These are termed edge-supported, composite, and solidly supported structures. The edge-supported structure consists of a simple film of piezoelectric plus thin electrodes. The composite structure has an additional nonpiezoelectric membrane layer. The fundamental frequency of both the edge-supported and composite structure is determined by the acoustic round-trip through the total thickness, implying similar overall thickness. The solidly mounted FBAR (SMR) [1] uses many alternating layers with high and low acoustic impedance as Bragg reflectors to realize the acoustic isolation and form the resonant cavity. This structure is favorable for integration, but needs strict thickness control of the reflection layers. Spurious responses near the resonant region are likely to be difficult to avoid in an SMR due to thickness variations in the reflection layers.

In this paper, the edge-supported structure was used to assess the performance of ZnO and PZT FBARs. In practice, for successful fabrication, additional thin layers must be incorporated into the simple membrane, making the structure nonsymmetrical. The extra layer is piezoelectrically inactive and acts as the mass loading layer on the FBAR, resulting in a lower effective coupling coefficient. For wide-band applications of FBARs, the thickness of the extra layer should be minimized. Ideally, the same fabrication that is used for individual FBARs can be used for FBAR filter construction. The following sections will show that this is possible.

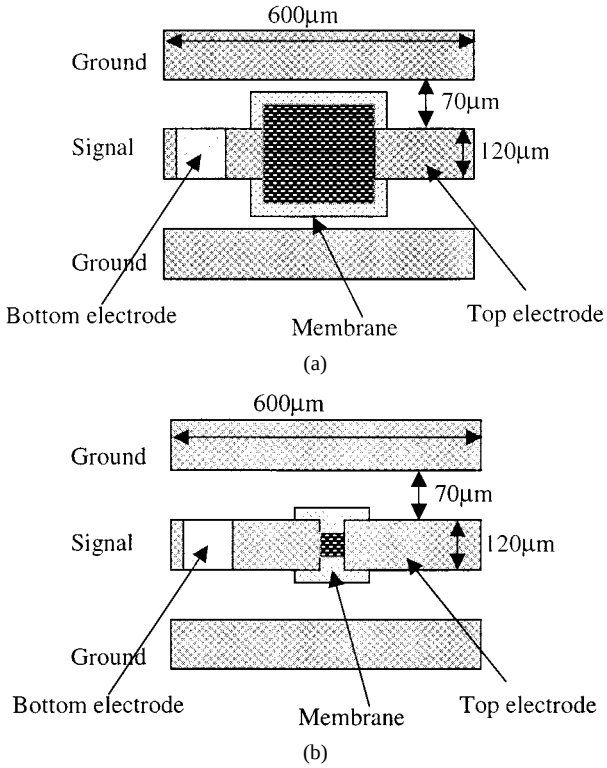

Fig. 2. Top view of: (a) ZnO FBAR and (b) PZT FBAR configured within CPW transmission lines.

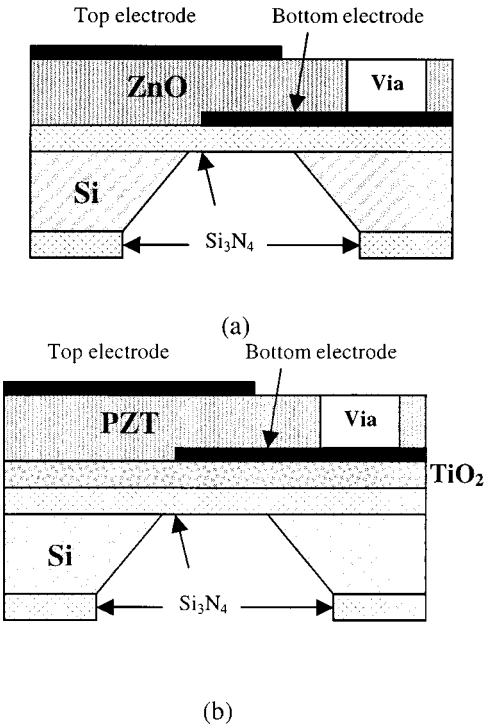

Fig. 3. Cross section of: (a) ZnO FBAR and (b) PZT FBAR.

III. ZnO AND PZT RESONATOR DESIGN

A. Coplanar-Waveguide Feeds

The use of coplanar transmission lines provides a very convenient method of making contact with a FBAR device [6]. Coplanar waveguides (CPWs) provide a well-defined ground plain and avoid the introduction of stray inductances, which arise when wire bonding is used. The avoidance of such parasitics with CPWs also simplifies FBAR modeling. On-wafer or on-die measurements are also easily performed using ground–signal–ground probes. The effects of any parasitic effects are easier to identify and measure if the characteristic impedance of the CPW, i.e., Z_0, matches the network analyzer input resistance and cable characteristic impedances of 50 Ω.

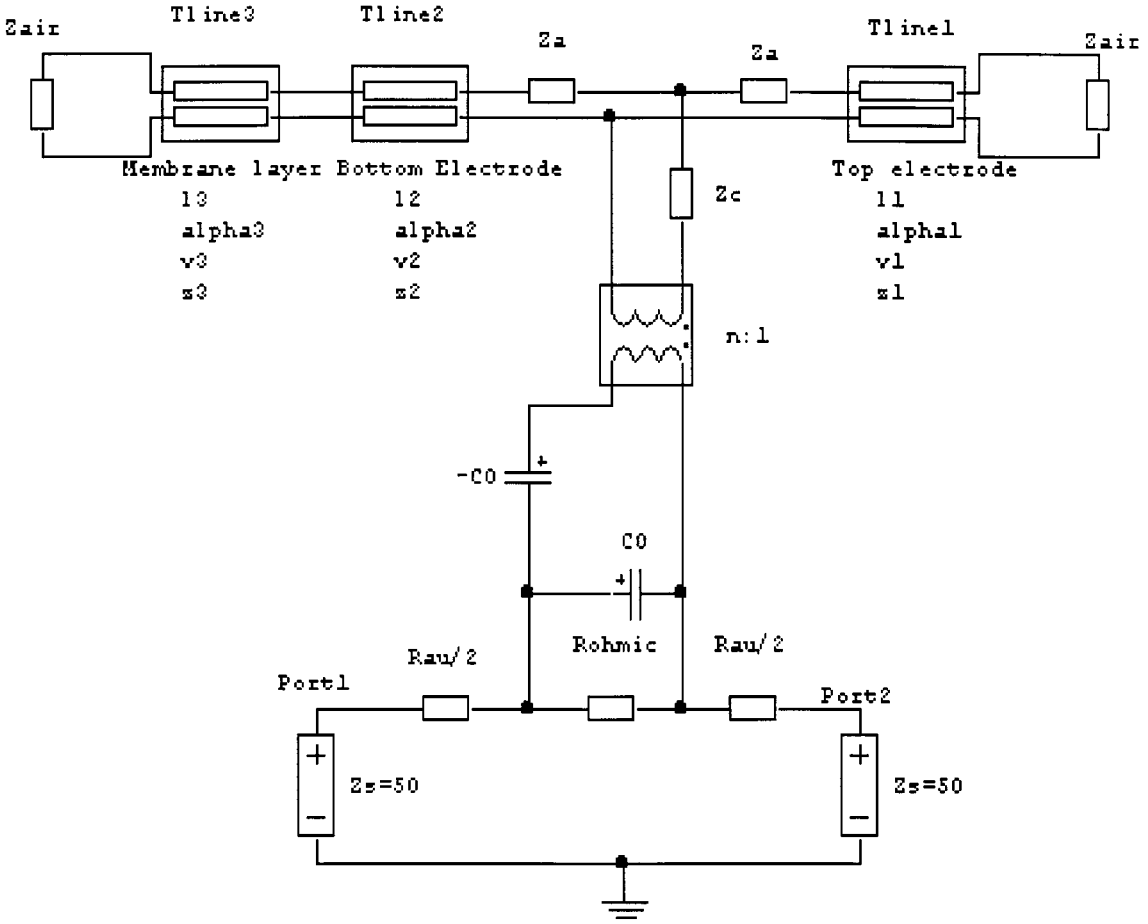

Fig. 4. Equivalent microwave circuit of composite FBAR.

It is important to assess the influence of the CPW on the measured FBAR device response. An accurate circuit representation of an FBAR located within a CPW is shown in Fig. 1. The S-parameters of this circuit can be calculated by cascading the transmission lines (with length of $L/2$, where L is the total length of CPW transmission line) and an FBAR. When the propagation constant γL is small, the following approximation is valid:

$$\sinh(\gamma L) \approx \gamma L$$
$$\cosh(\gamma L) \approx 1$$

Using these relations, it is possible to derive the following s-parameters:

$$S_{11} = \frac{Z + \dfrac{Z_0^2 - Z_S^2}{Z_0}(\gamma L)}{2Z_S + Z + \dfrac{ZZ_S + Z_0^2 + Z_S^2}{Z_0}(\gamma L)}$$
$$S_{11} = \frac{2Z_S}{2Z_S + Z + \dfrac{ZZ_S + Z_0^2 + Z_S^2}{Z_0}(\gamma L)} \quad (1)$$

where Z_0, Z_s and Z are the characteristic impedance of the transmission line, source impedance, and electrical impedance of FBAR, respectively. When $Z_0 = Z_s$, i.e., the characteristic impedance of CPW transmission line is the same as the source impedance Z_s

$$S_{11} = \frac{Z}{(2Z_S + Z)(1 + \gamma L)}$$
$$S_{21} = \frac{2Z_S}{(2Z_S + Z)(1 + \gamma L)} \quad (2)$$

The effect of the CPW transmission line can be neglected because $\gamma * L$ is small in our frequency range (1∼3 GHz). However, if $Z_0 \neq Zs$, the CPW transmission line will influence not only the magnitude of S_{11}, but also the series resonant frequency position, thus contributing to the overall FBAR response. Especially when the $\mathrm{Re}(Z_0) < Zs, S_{11}$ can be adjusted to be very small (∼80 dB) at the series resonance as the effect of the transmission line cancels out the real part of Z, while S_{21} is only slightly altered.

Ideally, the CPW connected to an FBAR would be 50 Ω. The dimensions of the CPW used in this paper were based on calculations to achieve 50 Ω for metal lines on a high-resistivity silicon substrate. Typical dimensions adopted are shown in Fig. 2. In our device design, the lines lie on the piezoelectric layer, which, although only 1-μm thick, has a high dielectric constant. Several calibration "through" transmission lines were fabricated on top of the material layers that make up the FBAR structure. For ZnO, which has a dielectric constant of $\varepsilon_r \sim 9$, 50-Ω transmission lines resulted and, thus, should not perturb the extrac-

tion of FBAR properties. The situation for PZT is more uncertain because of its high dielectric constant and will be the subject of more detailed measurements in the future.

B. ZnO and PZT Resonator Design

The area of a given resonator type determines its clamped capacitance value. For a given area, the clamped capacitance of a PZT FBAR will be much higher than a ZnO FBAR since the dielectric constant of PZT is much higher than ZnO. A high clamped capacitance obscures the resonance peak of the transmission coefficient S_{21}. A mask was produced having FBARs varying in area from 45 to 280 μm^2. Fig. 2(a) and (b) are schematics of the device layers of a ZnO FBAR and PZT FBAR, respectively, centered in a CPW.

IV. Fabrication of ZnO and PZT FBARS

Both ZnO and PZT FBARs were fabricated on high-resistivity silicon substrates to eliminate any parasitic contributions from mobile charges. A schematic of the ZnO and PZT FBAR layer structures is given in Fig. 3. For both structures, a Si_3N_4 (200 nm) layer served both as a support membrane and an etch barrier layer. PZT layers deposited on Si_3N_4 were found to have poor surface morphology, including cracks. A thin layer of TiO_2 ($\sim$50 nm) was inserted between the Si_3N_4 and PZT to avoid this cracking [7]. The metal electrode layers were 100-nm thick.

C-axis-oriented ZnO thin films were deposited by RF sputtering [8]. A sol-gel preparation [9] route was used for the PZT films. The PZT layer was formed by repeated spinning and baking of individual sol-gel layers. For FBAR fabrication, both ZnO and PZT layers were processed as blanket layers and the only patterning these layers required was the opening of large-area contact holes for access of the microwave probes. ZnO FBAR structures were prepared with Cr/Au electrodes, while Pt was used for PZT FBARs.

In the case of PZT FBAR structures, it is necessary to pole the PZT in the active area of the device. To avoid membrane rupture, poling must take place before membrane formation. Suitable contacts holes through the PZT were formed to allow access for poling voltages.

V. FBAR Measurement and Analysis

The most important filter design parameters are: 1) the frequency of the mode of interest; 2) the frequency spacing between the series and parallel resonances; 3) the loss in the resonator; and 4) the clamped capacitance of the resonator. The spacing between the series and parallel resonances and the acoustic loss are determined by the material constants of the layers that make up the acoustic stack. The effective coupling constant $\kappa^2_{t\,\mathrm{eff}}$ and device Q are defined as figures of merit to give a measure of the series to parallel resonance spacing and the acoustic loss of an FBAR, respectively.

As shown in Fig. 3, the FBAR structures used in this study consist of: 1) membrane and buffer layer; 2) bottom electrode; 3) piezoelectric layer; and 4) top electrode. Standard modeling for a composite FBAR starts with a one-dimensional Mason model, where nonpiezoelectric layers are treated as part of an acoustic transmission line [10]. The electrical impedance of the FBAR

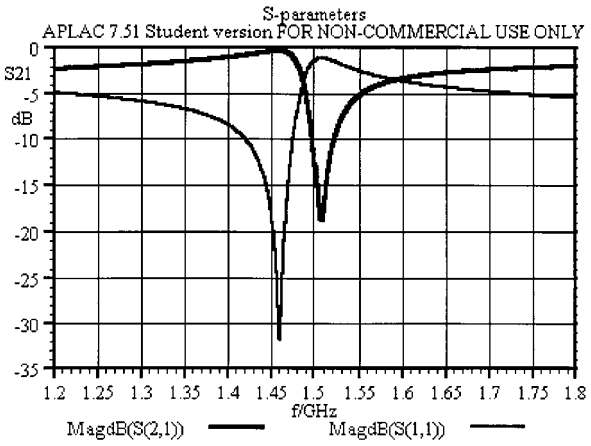

(a)

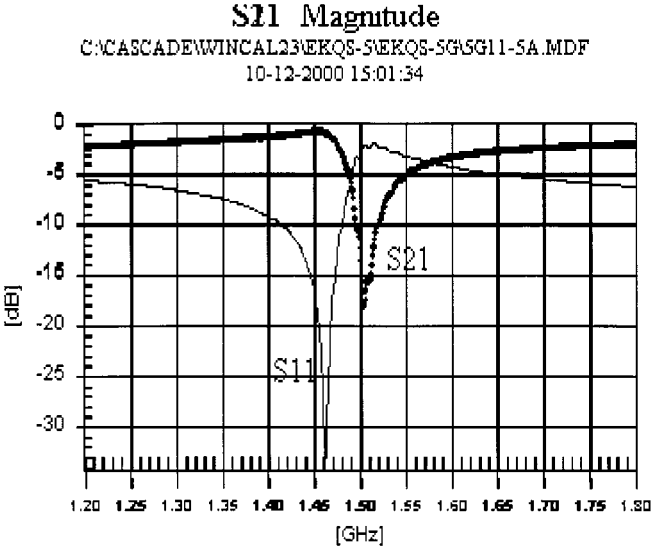

(b)

Fig. 5. (a) Comparison of modeled behavior for a ZnO FBAR. (b) Compared to experimental data.

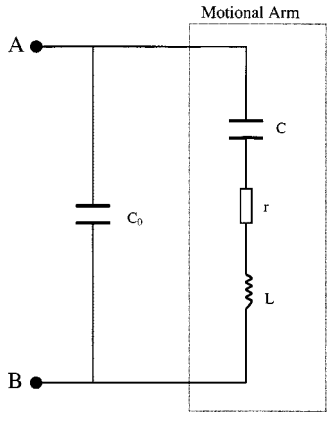

Fig. 6. BVD equivalent circuit of an FBAR.

is calculated and converted to predicted S-parameters. The full FBAR model used in this paper is shown in Fig. 4 and includes the acoustic loss in each layer; electrode losses, R_{au}, dielectric losses, and dc losses (R_{ohmic}) of the piezoelectric layer can

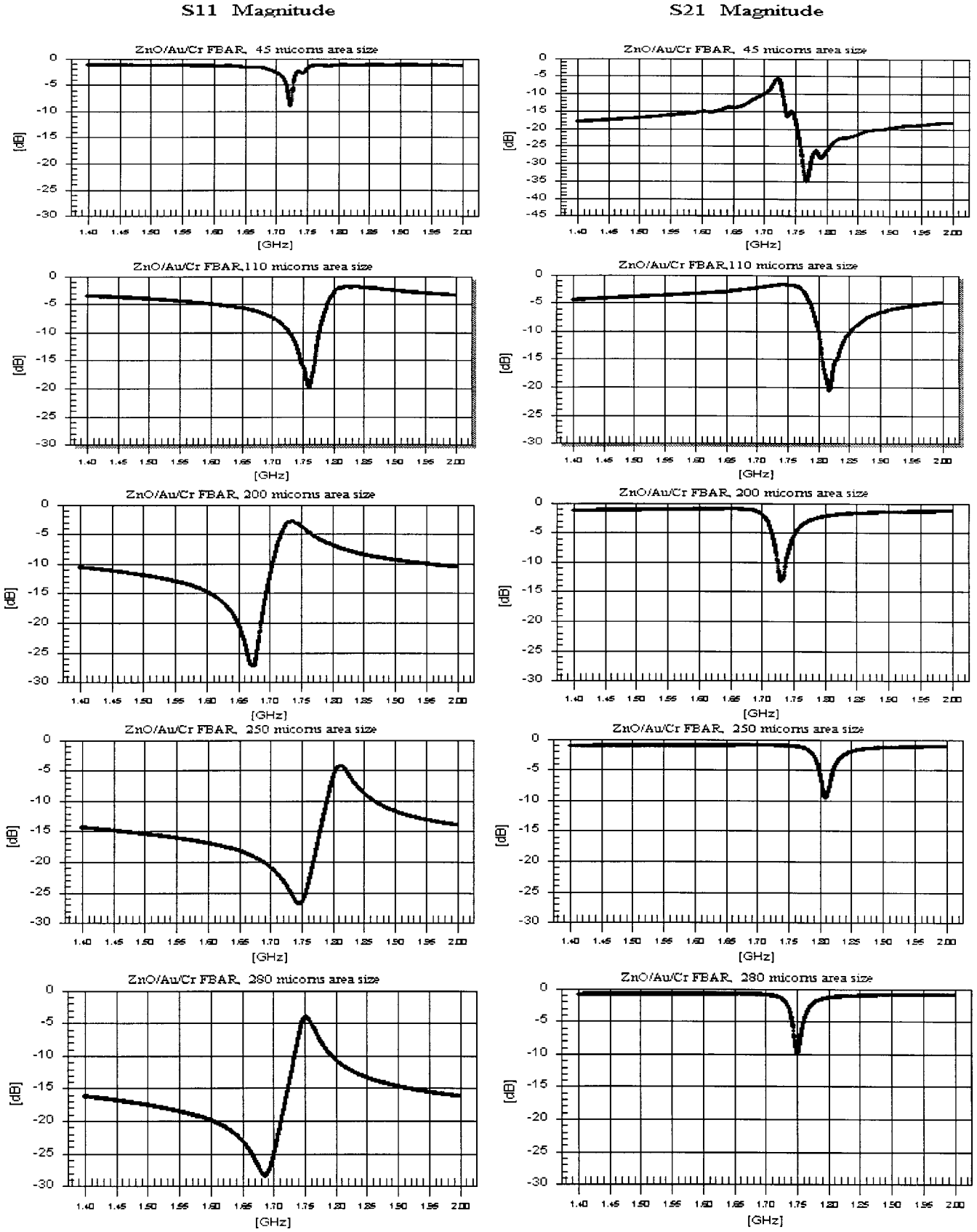

Fig. 7. S-parameters recorded from ZnO FBARs having areas from 45 to 280 μm^2.

also be included in the model. It is possible to calculate the S-parameters for this model using commercially available microwave software packages. Fig. 5 shows the result of simulation of a ZnO FBAR for a ZnO film thickness of 1.2 μm. The

ZnO acoustic parameters used in the model were taken from ZnO single crystal data [11], measured values were used for the thickness of the piezoelectric, barrier, and electrode layers. The acoustic properties of SiO_2 were used to represent the silicon nitride layer [4]. Fig. 5 reveals good agreement between modeled and experimental data.

A. Deduction of Q Values

The Q-value of an FBAR can be obtained from two-port S-parameters measurement. Fig. 6 shows the Butterworth–Van Dyke (BVD) circuit of the FBAR. The input impedance Z_{in} is

$$Z_{\text{in}} = \frac{-jX_{C0}[r + j(X_L - X_C)]}{r + j(X_L - X_C - X_{C0})} \tag{3}$$

where X_{C0}, X_C and X_L and r are the reactance of the clamped capacitor, motional capacitor, inductor, and resistance, respectively. At the parallel resonant frequency ω_p

$$X_L - X_C - X_{C_0} = 0$$
$$r \ll X_L - X_C$$

the impedance reaches its maximum value R. From (1), we can get R

$$R \approx \frac{X_{C0}(X_L - X_C)}{r} = \frac{X_{C0}^2}{r} = \frac{1}{r(\omega_p C_0)^2}. \tag{4}$$

The Q value at series resonant frequency Q_s is defined as

$$Q_s = \frac{1}{\omega_s C r}. \tag{5}$$

From (4) and (5), we have

$$R = \frac{\omega_s^2 C^2}{\omega_p^2 C_0^2} Q_s^2 r \tag{6}$$

since

$$\frac{\omega_p^2}{\omega_s^2} = \frac{C_0 + C}{C_0} = 1 + \frac{C}{C_0}. \tag{7}$$

(6) becomes

$$R = \left[\frac{\omega_p^2 - \omega_s^2}{\omega_p \omega_s}\right]^2 Q_s^2 r. \tag{8}$$

Therefore,

$$Q_s = \frac{\omega_p \omega_s}{\omega_p^2 - \omega_s^2}\sqrt{\frac{R}{r}} = \frac{\left(\frac{\omega_s}{\omega_p}\right)}{1 - \left(\frac{\omega_s}{\omega_p}\right)^2}\sqrt{\frac{R}{r}}. \tag{9}$$

R and r are the maximum and minimum value of impedance and can be obtained from the minimum values of S_{21} and S_{11}, respectively,

$$R = \frac{(1 - |S_{21\text{Min.}}|)}{|S_{21\text{Min.}}|} 2Z_s$$
$$r = \frac{|S_{11\text{Min.}}|}{(1 - |S_{11\text{Min.}}|)} 2Z_s \tag{10}$$

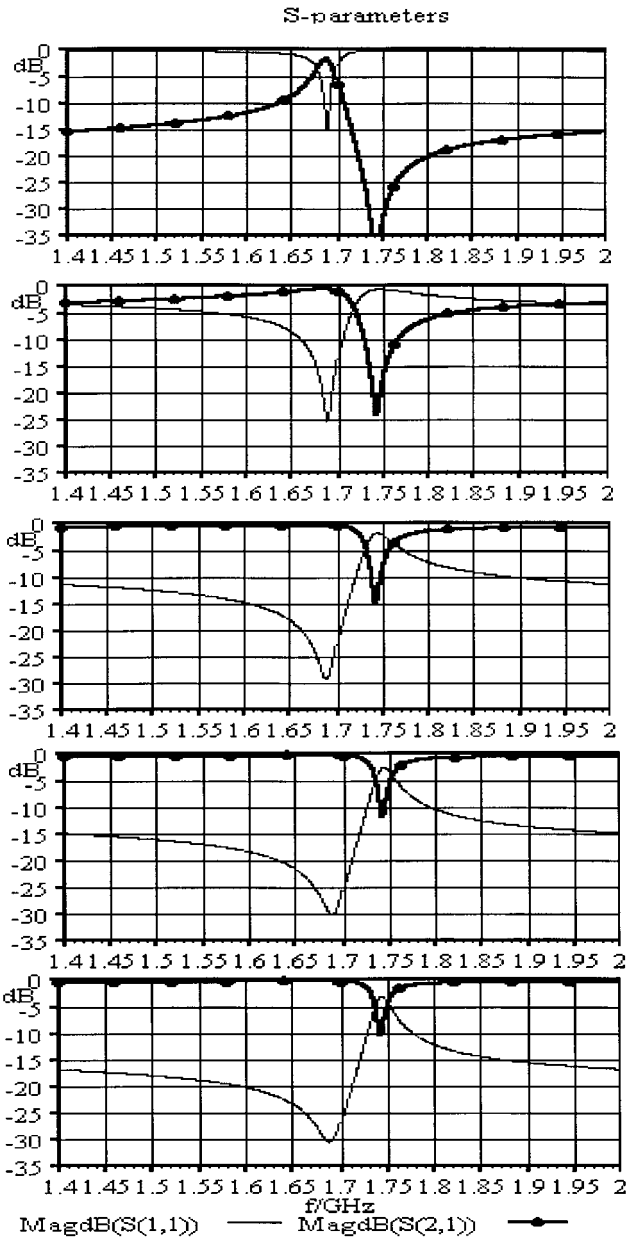

Fig. 8. Simulation of ZnO FBARs with different areas. From top to bottom: 45, 110, 200, 250, and 280 μm^2.

Where the Z_s is the source impedance 50 Ω. From (7) and (8), the Q value of the FBAR can be obtained from S-parameter measurements

$$Q_s = \frac{\left(\frac{\omega_s}{\omega_p}\right)}{1 - \left(\frac{\omega_s}{\omega_p}\right)^2}\sqrt{\frac{(1 - |S_{21\text{Min.}}|)}{|S_{21\text{Min.}}|}\,\frac{(1 - |S_{11\text{Min.}}|)}{|S_{11\text{Min.}}|}}. \tag{11}$$

The advantage of this method for determining Q is that the derivation takes full account of acoustic and electrical loss mechanisms. From the above equation, the obtained Q value of ZnO FBAR in Fig. 5(b) is $\sim$350.

B. ZnO FBAR Results and Analysis

Fig. 7 shows S-parameter results obtained from ZnO FBARs whose device area varied from 45 to 280 μm^2. As previously

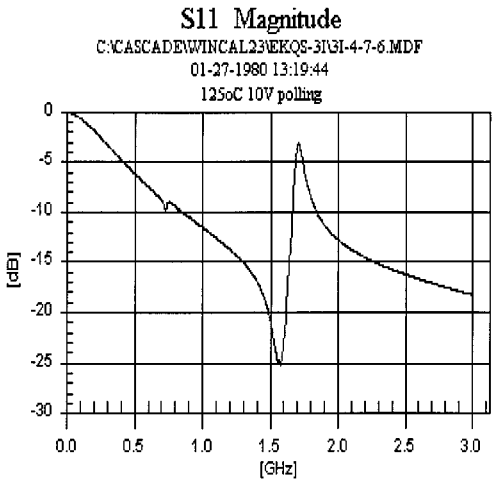

(a)

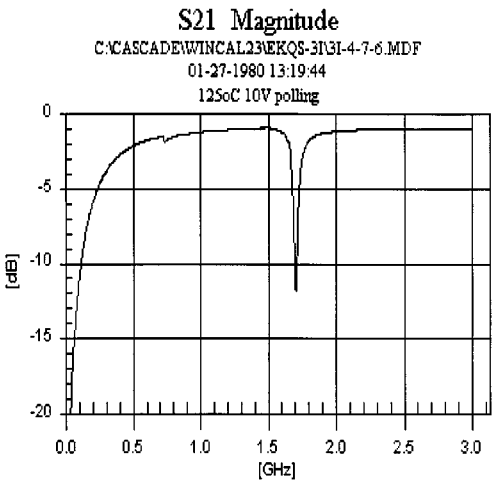

(b)

Fig. 9. S-parameters recorded from a PZT FBAR having an area of 45 μm^2.

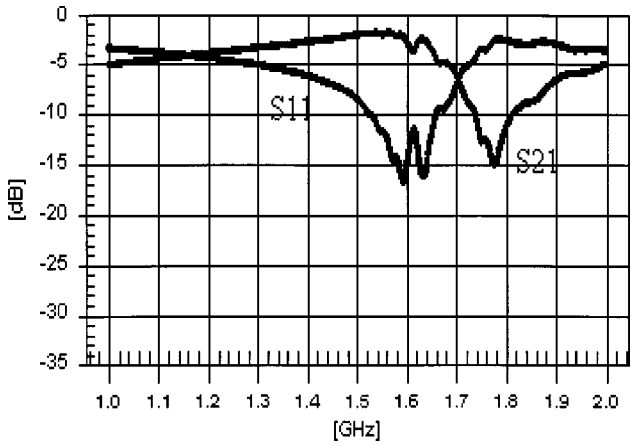

(a)

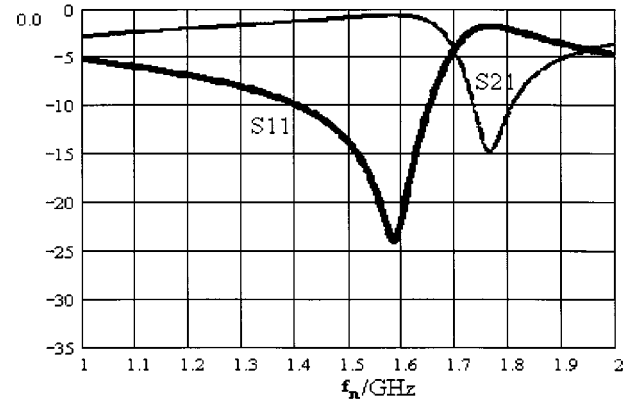

(b)

Fig. 10. (a) S-parameters recorded from a small area PZT FBAR. (b) Compared to the predicted response.

discussed, an increase in the area of the resonator leads to an increase in the minimum value of S_{21} due to the increase in the value of the clamped capacitance. This is evident from (2) and (8). The simulated results using the material values listed in Table I are shown in Fig. 8. The agreement between modeled and measured data is very good and suggests that the equivalent circuit is providing an accurate representation of the resonator. The agreement for the smallest area FBAR is not so good because of the appearance of extra spurious resonances that lower the Q value of the pure extensional resonance. A more sophisticated model would be necessary to take account of these extra resonances [12]. It is also possible to calculate a value for the electromechanical coupling coefficient κ_t^2. For our ZnO FBARs, κ_t^2 is $\sim$7%, which is very close to the bulk value of ZnO, which is 7.84% [11].

C. PZT FBAR Results and Analysis

The circuit model developed for the ZnO FBAR was used to model PZT FBAR data. For PZT thin films, the material parameters are not well established, and part of the purpose of this paper is to obtain values for the coupling coefficients. Fig. 9 shows recorded S-parameters from a poled 45-μm^2 PZT FBAR. The PZT layer thickness was 0.75 μm. Typical poling voltages used were 15 V, applied for 1–3 min at 125 °C. Using (9), a Q value of this resonator is estimated to be $\sim$54. The electromechanical coupling coefficient κ_t^2 can be estimated from the resonant frequencies ω_s and ω_p, as well as from the modeled equivalent circuit. A value of $\kappa_t^2 \approx 19.8\%$ is obtained, which is close to the value that would be expected for the bulk ceramic PZT [4].

Fig. 10(a) reveals strong spurious responses measured within the resonance region on a small-area 20-μm^2 PZT FBAR. Such responses are probably responsible for the deviation of the measured and modeled data [see Fig. 10(b)]. It is probable that such spurious resonances are also responsible for the substantial difference between modeled and measured data for the small-area ZnO FBAR, as revealed in Figs. 7 and 8.

VI. FBAR Filters

There have been several approaches to constructing FBAR filters [6]. In this paper, we have investigated the ladder filter configuration, which uses series and shunt FBARs. To design such filters, we have used the equivalent-circuit representation previously described for both ZnO and PZT FBARs, as well as the material properties derived from the analysis of single FBARs using these models.

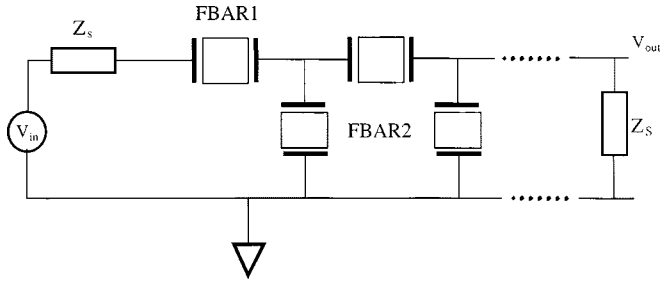

Fig. 11. Equivalent circuit of an FBAR ladder filter.

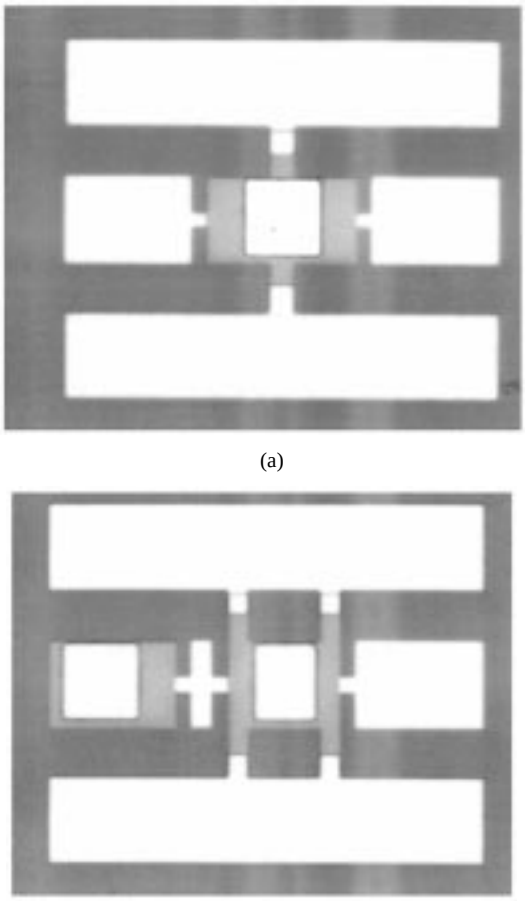

(a)

(b)

Fig. 12. Optical image of fabricated: (a) 2 × 2 and (b) 3 × 4 PZT FBAR filters.

A. Modeling of FBAR Filters

Fig. 11 shows the equivalent circuit of a FBAR ladder-type filter consisting of series and shunt FBARs. An FBAR ladder filter can be designated as $A \times B$, where A is the number of series FBAR elements and B is the number of shunt FBAR elements. A simple way to calculate the transmission coefficient S_{21} is to use the chain parameters. For a series FBAR, the chain matrix is

$$\mathbf{M}_s = \begin{pmatrix} 1 & Z_1 \\ 0 & 1 \end{pmatrix} \tag{12}$$

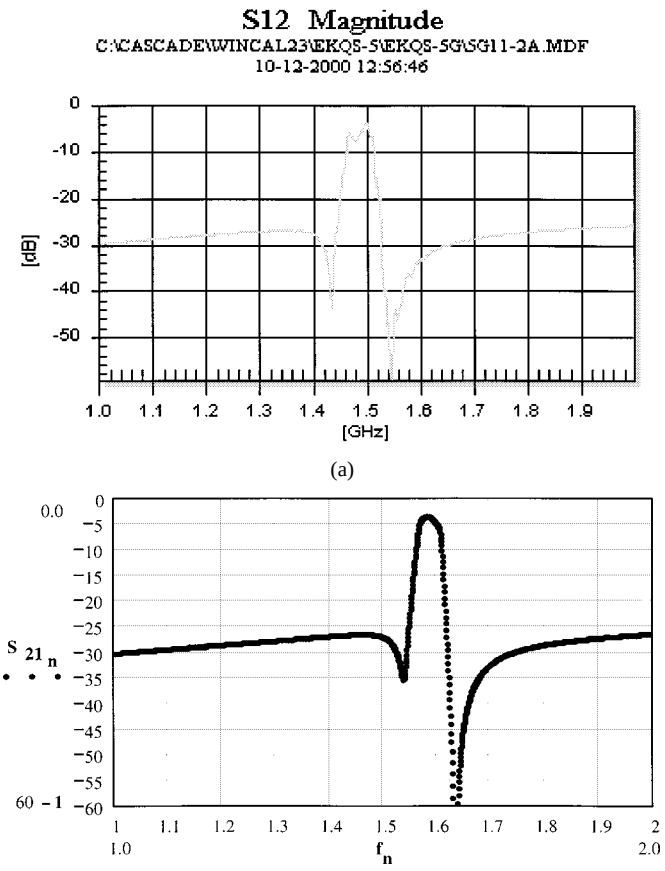

(a)

(b)

Fig. 13. Recorded S-parameters: (a) from a 2 × 2 ZnO FBAR compared to (b) the predicted modeled behavior.

where Z_1 is the electrical impedance of a series FBAR derived from equivalent-circuit modeling. The chain matrix for the shunt FBAR is

$$\mathbf{M}_p = \begin{pmatrix} 1 & 0 \\ Y_2 & 1 \end{pmatrix} \tag{13}$$

where Y_2, the admittance of a shunt FBAR is the inverse of the impedance $Y_2 = 1/Z_2$. The total chain matrix $\mathbf{M}$ can be obtained by multiplying all $\mathbf{M_s}$ and $\mathbf{M_p}$ as follows:

$$\mathbf{M} = \begin{pmatrix} \mathbf{A} & \mathbf{B} \\ \mathbf{C} & \mathbf{D} \end{pmatrix} = \mathbf{M}_s\mathbf{M}_p \bullet \bullet \bullet \bullet. \tag{14}$$

Therefore, the S_{21}–parameters of this circuit are given by

$$\mathbf{S}_{21} = \frac{2 \times Z_s}{\mathbf{A} \times Z_s + \mathbf{B} + \mathbf{C} \times Z_s \times Z_s + \mathbf{D} \times Z_s}. \tag{15}$$

The insertion loss of a ladder filter is determined not only by the Q value of each FBAR, but also by the accuracy with which the resonant frequencies of series and shunt FBARs can be modeled and achieved experimentally. The smallest insertion loss is obtained when the parallel resonance frequency of the shunt FBAR is adjusted to be equal to series resonance frequency of the series FBAR. This can be achieved by adjusting the thickness of any of the layers within the shunt FBARs. The out-of-band rejection is determined by the S_{11} of the series FBARs and the S_{21} of the shunt FBARs. From Figs. 6 and 7, it

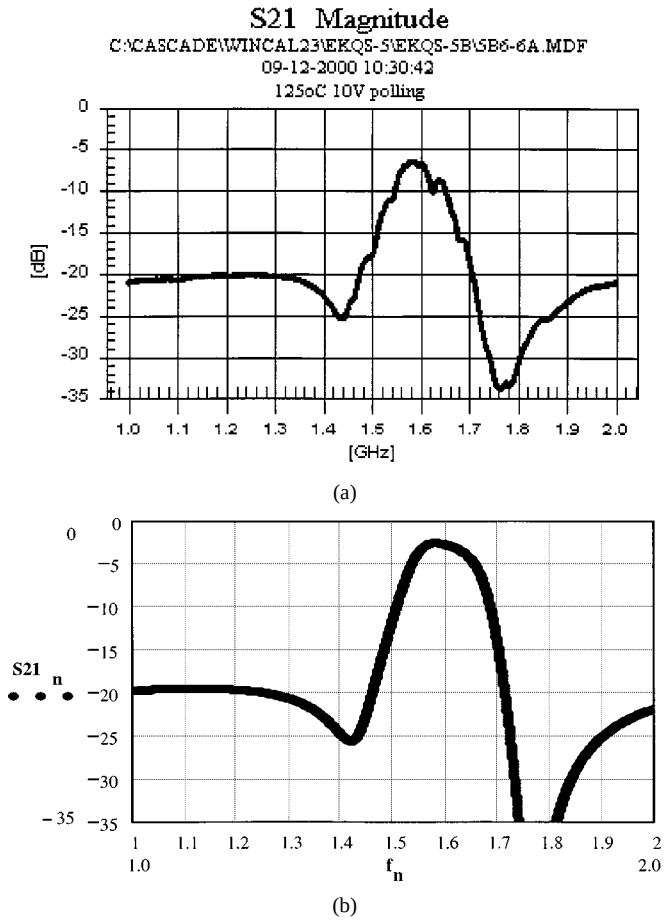

Fig. 14. Measured transmission coefficients: (a) for a 2 × 2 PZT FBAR filter compared to (b) predicted behavior.

is apparent that a smaller area for the series FBARs and a larger area for the shunt FBARs will help to increase the out-of-band rejection. Therefore, series and shunt FBARs having different areas in the FBAR ladder filter is a design variable.

B. Filter Fabrication and Results

The FBAR filter fabrication processes and their sequences are very similar to those used to fabricate the single FBAR shown in Fig. 2, except now, several resonators are formed on a single membrane. Different resonant frequencies for the series and shunt structures was achieved by using different electrode thickness. This involved using separate liftoff processes for the metallizations of the shunt and series elements.

Fig. 12 shows images of fabricated 2 × 2 (two series and two shunt FBARs) and 3 × 4 (three series and four shunt FBARs) PZT FBAR filters. Generally, the filters are small, and even higher order filters can be placed within a 600-μm^2 membrane.

Fig. 13 compares the modeled and experiment results for a 2 × 2 ZnO filter. As previously mentioned, the designed FBAR performance is based on modeled parameters derived from the analysis of single FBARs. The measured insertion loss of the fabricated ZnO filter is higher than the modeled design value. This can be attributed to deviations in the resonant frequencies of FBARs from the designed values, i.e., the parallel resonance frequency of the shunt FBAR is not exactly the same as the series resonance frequency of the series FBAR. In this situation, the minimum value of S_{21} for the shunt FBAR does not occur at the same frequency as the maximum value of S_{21} for the series FBAR. In this situation, additional signal power will leak through the shunt FBAR, increasing the insertion loss.

Fig. 14 shows the modeled and experimental results for a 2 × 2 PZT FBAR filter. The predicted modeled filter performance was based on experimental data from a FBAR, which showed no spurious resonator responses. The measured passband insertion loss and the close-in rejection differ considerably from the design values. An insertion loss of ∼6.5 dB is measured compared to the predicted 2.5 dB. Possible reasons include those already discussed for ZnO FBAR filters, where the resonant frequencies for the series and shunt elements differ from their designed values. Measurements on process control resonators did, in fact, reveal deviations from design frequencies; however, the difference is not sufficient to explain all of the extra insertion loss. Another contribution to the increased loss is the lowering of the Q value due to spurious responses. The spurious resonances' losses are particularly high for PZT FBARs having small area.

Comparing ZnO and PZT FBAR filters, larger 3-dB bandwidths can be obtained for a PZT FBAR filter, as shown by comparing Figs. 13 and 14. Depending on the exact filter design, 3-dB bandwidth of ∼60 and ∼120 MHz can be expected for ZnO and PZT FBAR filters, respectively.

VII. Conclusions

Processes were developed for fabricating both ZnO and PZT FBAR structures. Both ZnO and PZT FBARs were fabricated and their frequency responses compared. Typical Q values of ∼350 for ZnO FBARs and 54 for PZT FBARs were obtained. An equivalent microwave-circuit model was developed that could accurately model composite FBAR performance. A value of $\kappa_t^2 \approx 19.8\%$ was obtained for the effective coupling coefficient of thin-film PZT.

Bandpass ladder filters were designed using ZnO and PZT FBAR data. Both ZnO and PZT filters were fabricated having ∼60- and ∼100 –MHz 3-dB bandwidths, respectively, at ∼1.5 GHz. The larger bandwidth for PZT results from the larger electromechanical coupling coefficient of PZT compared to ZnO and confirms that PZT FBARs and FBAR filters are promising candidates for future wide-band application, especially if the losses can be reduced. Compared to the designed filter performance, a higher insertion loss was observed in the fabricated FBAR filters, which was attributed to the deviation of the resonant frequencies of the used FBARs compared to the designed values, as well increased loss due to spurious responses from FBARs with smaller area.

References

[1] K. M. Lakin, "Thin-film resonators and filters," in *Proc. IEEE Ultrason. Symp.*, 1999, pp. 895–906.
[2] S. V. Kirshnawary, J. F. Rosenbaum, S. S. Horwitz, and R. A. Moore, "Film bulk acoustic wave resonator technology," in *Proc. IEEE Ultrason. Symp.*, vol. 1, 1990, pp. 529–536.
[3] L. Mang, F. Hickernell, R. Pennell, and T. Hickernell, "Thin-film resonator ladder filter," in *IEEE MTT-S Int. Microwave Symp. Dig.*, vol. 2, May 16–20, 1995, pp. 887–890.
[4] V. M. Ristic, *Principles of Acoustic Devices*. New York: Wiley, 1983.

[5] P. Muralt, "PZT thin films for microsensors and actuators: Where do we stand?," *IEEE Trans. Ultrason., Ferroelect., Freq. Contr.*, vol. 47, pp. 903–915, July 2000.
[6] S. V. Krishnaswamy, S. S. Horwitz, and R. A. Moore, "Microwave film bulk acoustic resonator and manifold filter bank," U.S. Patent 5 185 589, Feb. 9, 1993.
[7] P. B. Kirby, R. V. Wright, P. Gaucher, P. Galtier, L. Kofoed, J. O. Gullov, W. Von Munch, D. Eichner, B. Ploss, and J. K. Kruger, "Report on Brite–EuRam programme SEMDEFT," in *2nd European Integrated Ferroelect. Meeting*, Jouy-en Josas, France, Sept. 29–30, 1997, pp. 161–169.
[8] E. Komuro, Q. Su, Z. Huang, P. B. Kirby, and R. W. Whatmore, "Effect of electrodes on GHz ZnO thin film bulk-acoustic-wave resonator," in *12th Int. Integrated Ferroelectr. Symp. Dig.*, Aachen, Germany, Mar. 12–15, 2000, pp. 434–440.
[9] Z. Huang, Q. Zhang, and R. W. Whatmore, "Low temperature crystallization of lead zirconate titanate thin films by a sol-gel method," *J. Appl. Phys.*, vol. 85, no. 10, pp. 7355–7361, 1999.
[10] K. M. Lakin, "Modeling of thin-film resonators and filters," in *IEEE MTT-S Int. Microwave Symp. Dig.*, vol. 1, 1992, pp. 149–152.
[11] J. F. Rosenbaum, *Bulk Acoustic Wave Theory and Devices*. Norwood, MA: Artech House, 1988, pp. 144–147.
[12] P. T. Tikka, J. Kaitila, J. Ella, T. Makkonen, J. V. Knuuttila, J. Westerholm, and M. M. Salomaa, "Laser probing and FEM modeling of solidly mounted resonators," in *IEEE MTT-S Int. Microwave Symp. Dig.*, vol. 199, pp. 1373–1376.

Qing-Xin Su received the B.E. degree in material science from Tsinghua University, Beijing, China, in 1989, studied high-Tc superconducting thin films at the Institute of Physics, Chinese Academy of Sciences, Beijing, China, and received the Ph.D. degree in ferroelectric thin films from the Hong Kong University of Science and Technology, Hong Kong, in 1995.

He was a Post-Doctoral Fellow in the Electrical and Computer Engineering Department, Rice University, where, from 1995 to 1998, he was involved in the area of ferroelectric thin-film capacitors and LiNbO3 thin-film SAW devices. He then joined Cranfield University, Cranfield, Bedford, U.K., as a Research Officer, where he was involved with film bulk acoustic wave resonators (FBARs). He is currently a Project Leader with Philips Research East Asia-Xi'an, Xi'an, China, where he is involved in the area of RF subsystem design for 3G mobile and bluetooth applications. His main interest is focused on SAW/FBAR filter design, RF/microwave circuit design, and analysis for wireless communication and sensor application. He has authored or co-authored over 20 technical papers.

Paul Kirby received the Ph.D. degree from the University of Cambridge, Cambridge, U.K., in 1979.

He was with the IBM Thomas J. Watson Research Center, New York, NY, Harvard University, Cambridge, MA, and GEC Hirst Laboratory, London, U.K., and Caswell Laboratory, Towcester, U.K. He is currently a Senior Lecturer of microsystems at Cranfield University, Cranfield, Bedford, U.K. His research interests include high-frequency microelectromechanical devices, thin-film SAW devices for remote-sensing applications and sputtering of functional thin films.

Eiju Komuro received the B. Eng., M. Eng., and Eng.D. degrees from the Tokyo Institute of Technology, Tokyo, Japan, in 1990, 1992, and 1995, respectively.

He then joined the Electronic Chemistry Department, Tokyo Institute of Technology, where he researched Bi-substituted garnet. In 1995, he joined the TDK Corporation. In April 1998, he joined Cranfield University, Cranfield, Bedford, U.K., where he is currently a Visiting Scientist. He is now studying the preparation and evaluation of dielectric thin films.

Masaaki Imura received the B.S., M.S., and Dr.E. degree in material science from Tohoku University, Tohoku, Japan, in 1991, 1993 and 1996, respectively.

In 1996, he joined the TDK Corporation. He is currently developing thin-film bulk acoustic resonator and filter technology in the Nanotechnology Group, Cranfield University, Cranfield, Bedford, U.K.

Qi Zhang received the B.Sc. degree in chemistry and the M. Eng. in materials science from the Wuhan University, Wuhan, China, in 1978 and 1986, respectively, and the Ph.D. degree from Monash University, Melbourne, Australia, in 1995.

He was with the Sol-gel Chemistry, Inorganic and Organic Chemistry Departments, Monash University. In 1996, he joined the Nanotechnology Group, Cranfield University, Cranfield, Bedford, U.K., as a Research Officer, where he continued his research into thin-film preparation by sol-gel processing. These thin-film materials mainly include complex metal oxides with ferroelectric and piezoelectric properties. In 1999, he became a Senior Research Fellow in this same group. He has authored or co–authored 40 journal and conference papers. His main areas of research are within inorganic and organic synthesis, particularly moisture-sensitive compounds such as metal alkoxides. His research also includes colloid chemistry, light scattering technology, and structural characterization of ferroelectric thin films using a range of analytical, optical, and electrical characterization techniques.

Roger Whatmore received the Ph.D. degree from Cambridge University, Cambridge, U.K., in 1976.

He was with the Cavendish Laboratory, Cambridge University, where he conducted original research into the structure and phase transitions in low-Ti content Pb(Zr,Ti)O3 solid solutions. In 1976, he joined GEC Marconi Materials Technology (formerly Plessey Research), Caswell, U.K., where he was involved with the applications of ferroelectric materials to piezoelectric, pyroelectric, and electrooptic devices. In October 1994, he took up the Royal Academy of Engineering Chair in Engineering Nanotechnology at Cranfield University, Cranfield, Bedford, U.K., where he is currently exploring the applications of ferroelectrics in microsystems and nanotechnology. He has authored or co-authored over 140 publications and holds 25 patents in the field of ferroelectric materials and their applications.